

RESEARCH ARTICLE

Biomechanical evaluation of an anatomical bone plate assembly for thin patella fracture fixation fabricated by titanium alloy 3D printing

Chi-Yang Liao^{1,2,3}, Shao-Fu Huang^{1,4}, Wei-Che Tsai¹, Yu-Hui Zeng¹, Chia-Hsuan Li^{1,4}, and Chun-Li Lin^{1,4*}¹Department of Biomedical Engineering, National Yang Ming Chiao Tung University, Taipei, Taiwan²Department of Orthopedics, Tri-Service General Hospital Songshan Branch, National Defense Medical Center, Taipei, Taiwan³Department of Surgery, Tri-Service General Hospital Songshan Branch, National Defense Medical Center, Taipei, Taiwan⁴Medical Device Innovation and Translation Center, National Yang Ming Chiao Tung University, Taipei 112, Taiwan

Abstract

This study established and evaluated the feasibility of a three-dimensional (3D)-printed titanium anatomical surface with adjustable thin bone plate assembly (AATBP) for patella fracture fixation. The AATBP was 1.6 mm in thickness and divided into a proximal plate (PP) with locking screw holes and a distal plate (DP) (0.4 mm in thickness) with compressive screw holes for assembly using a ratchet mechanism to adjust the total fixation height according to the patella size. Two pairs of hooks were designed on the proximal/distal edges to allow passage through the tendon to grip the fractured fragments. 3D printing combined with Computer Numerical Control (CNC) drilling was performed to manufacture the AATBP. Four-point bending and surface roughness tests were performed to evaluate the AATBP mechanical behavior. A cyclic (300 times) load test with 15-kg weights was adopted to compare the biomechanical stability between the AATBP and conventional tension band wiring (TBW) fixations. A parallel finite element (FE) analysis was achieved to understand the fracture gap and bone stress in the two different fixations on a transverse patella fracture. The result showed that the maximum AATBP manufacturing error was 3.75%. The average fracture gaps on the medial/lateral sides after cyclic loads were 2.38 ± 0.57 mm/ 2.30 ± 0.30 mm for TBW and 0.03 ± 0.01 mm/ 0.06 ± 0.03 mm for AATBP fixations. The same trend occurred in the FE simulation. This study confirmed that a complicated thin bone plate, including the anatomical surface, hooks, and ratchet with size-adjustable characteristics, can be fabricated using metal 3D printing with acceptable manufacturing error and reasonable anatomical surface/thin bone plate assembly fitness. Biomechanical cyclic tests and FE simulation showed that the AATBP fixation is superior to the conventional TBW for patella transverse fractures.

Keywords: Metal 3D printing; Anatomical surface; Assembly; Patella fracture; Bone plate

***Corresponding author:**Chun-Li Lin
(cllin2@nycu.edu.tw)

Citation: Huang S-F, Tsai W-C, Zeng Y-H, *et al.*, 2023, Biomechanical evaluation of an anatomical bone plate assembly for thin patella fracture fixation fabricated by titanium alloy 3D printing. *Int J Bioprint*, 9(6): 0117. <https://doi.org/10.36922/ijb.0117>

Received: April 5, 2023**Accepted:** June 17, 2023**Published Online:** July 18, 2023**Copyright:** © 2023 Author(s).

This is an Open Access article distributed under the terms of the Creative Commons Attribution License, permitting distribution, and reproduction in any medium, provided the original work is properly cited.

Publisher's Note: AccScience Publishing remains neutral with regard to jurisdictional claims in published maps and institutional affiliations.

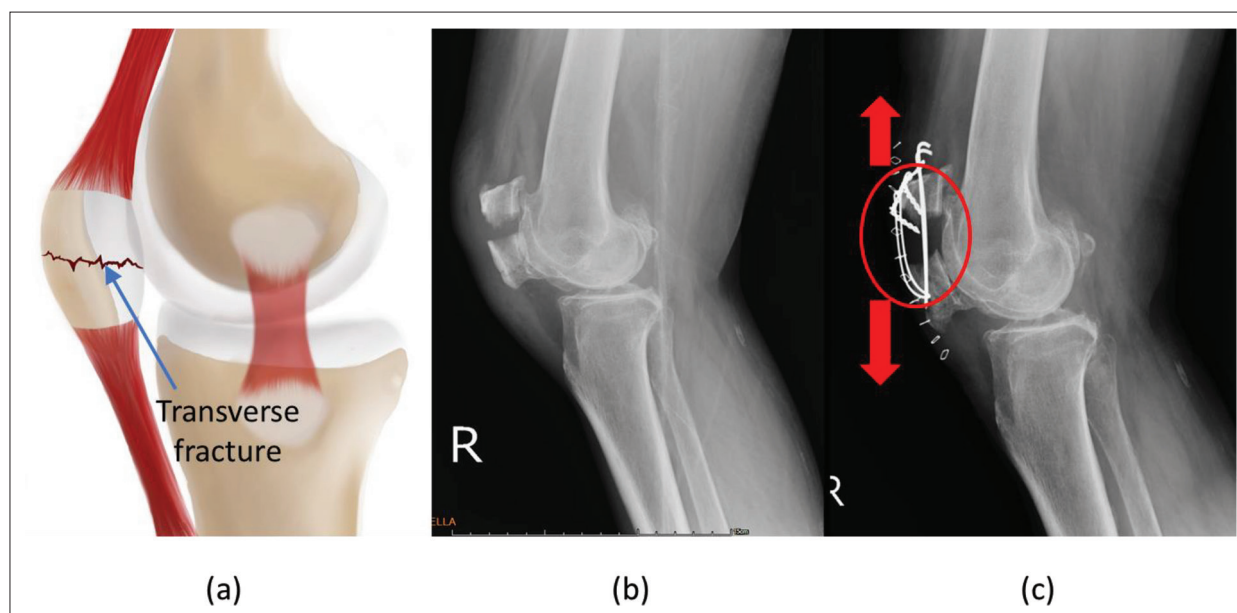


Figure 1. (a) Illustration of transverse fracture of the patella. (b) X-ray image of transverse fracture of the patella before surgery. (c) Fractured fragments cannot be fixed stably, and a gap was generated 2 weeks after surgery using a conventional band wire.

1. Introduction

Transverse fractures are the most common type of patella fractures in those aged between 30 and 60 years old^[1-5]. Surgical intervention with anterior tension band wiring (TBW) (using K-wires directly or cannulated lag screws) is necessary to reposition the articulating surface, achieve early mobilization, and reconstruct extensor function. However, clinical complications including fixation failure, migration, and skin irritation arise, requiring revision surgery with implant removal in up to 65% of cases^[4,6-8]. Although a bilateral fixed-angle plate was introduced to provide greater stiffness and lower fracture gap dehiscence for transverse patella fractures^[3], problems emerged with inaccurate pre-bending and alignment, bone screw interference, and lack of holding power for bone fragments^[4].

As the patella functions as a transmitter of tensile forces generated by the quadriceps muscles and as an effective lever arm for the knee extensor mechanism, patella integrity is crucial for proper knee function and physiological locomotion^[9]. The enormous tensile force on the patella generated by the quadriceps and patellar tendons cannot restore the fracture fragments effectively, representing the key failure in surgical treatment using traditional band wire fixation (Figure 1)^[3,4,10].

In a suitable patella fracture fixation plate design, there is a need to ensure enough holding power to effectively restore and fix the proximal and distal fractured fragments. It has been suggested that a hook mechanism should be

used while providing a compressive effect on the fractured bone fragments to maintain structural stability^[11,12]. Moreover, the anatomical shape and adjustable size need to be considered for patella anterior surface fitness and variation in size. It is essential that the fixation bone plate be designed as thin as possible to avoid clinical irritation because the patella is very close to the skin. Whether these complicated mechanical structures can be processed using three-dimensional (3D) printing is an important issue to be resolved.

This study developed a titanium 3D-printed anatomical contour bone plate with hook mechanisms and size adjustable assembly thin bone plates (AATBP) for patella fracture fixation. The anatomical surface/thin bone plate assembly fitness, manufacturing error, and bending/surface roughness tests for the AATBP were evaluated to understand the capability of metal 3D printing and bone plate mechanical behavior. Cyclic load tests and finite element (FE) analysis were performed to compare the biomechanical stability between this specifically designed osteosynthesis system and the conventional anterior TBW for use on transverse patella fractures.

2. Materials and methods

2.1. AATBP design

We designed a fractured patella fixation bone plate and noted an AATBP with a fixed medial-lateral width and adjustable height in the proximal-distal direction with an anatomically curved surface. The AATBP anatomical

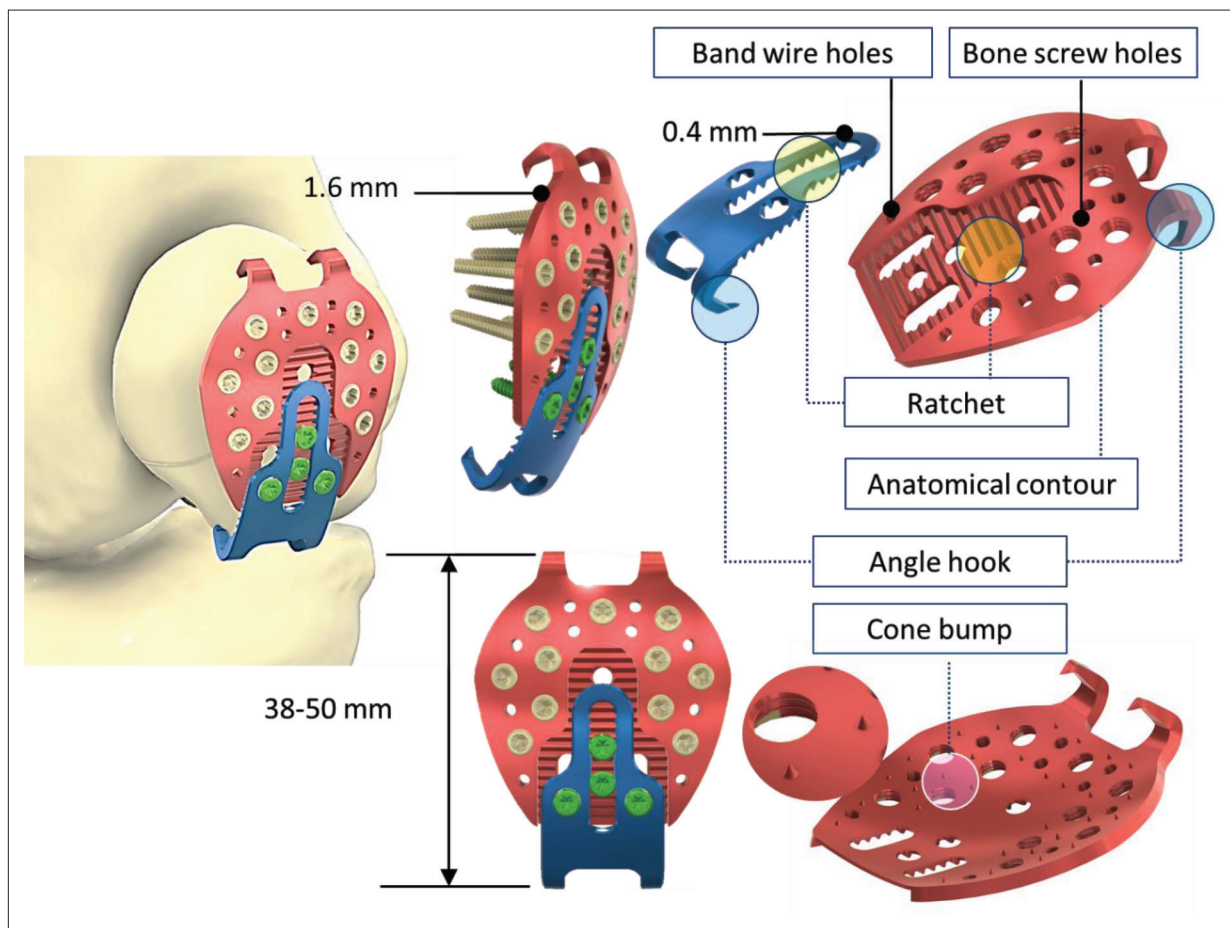


Figure 2. AATBP design concept with an anatomical curved surface of 1.6-mm thickness, including a DP with 0.4-mm thickness to ratchet onto the proximal plate (PP) for height adjustment.

curved surface was intended to adaptively fit to the patella surface curvature. The curved surface was obtained using a standard artificial patella made of polyurethane foam (Sawbones; Pacific Research Laboratories Inc., Vashon, WA, USA). This was used to capture the patella surface via a computed tomography (CT) scan, followed by reconstruction in image processing software (Mimics 22.0; Materialize NV, Leuven, Belgium). The AATBP thickness was designed to be 1.6 mm, which was divided into two thin pieces at the proximal and distal parts. The distal plate (DP; 0.4 mm in thickness) can be ratcheted and assembled onto the center of the proximal plate (PP). These two plates can be adjusted to extend the fixation total height from 38 to 50 mm to fit the relative positions according to the patella size (Figure 2).

Two pairs of hooks were designed onto the DP and PP edges that can pass through the tendon to grip the fractured patella fragments. Eleven locking and two compressive screw holes (2.4 mm in diameter) with medial–lateral symmetry in the PP and DP, respectively, were also created

to allow selective bone screw insertion to fix the AATBP to the fractured patella. A straight slot in the DP was also designed to allow the screw insertion accompanied by the adjustment of AATBP height. Ten 1.5-mm wire holes were created in the PP to allow the band wire to pass through, thereby enhancing the fixation capability when necessary. Cone bumps with a height of 0.6 mm were designed and randomly distributed onto the back of the PP, i.e., the surface contacting the bone surface, to increase bone plate and patella retention (Figure 2).

To verify the AATBP anatomical surface design feasibility, we randomly selected two males (48 and 71 years old) and one female (74 years old) from the CT database and reconstructed their complete and normal patella image models. The AATBP and three normal patella models were imported into CAD software (PTC Creo V6.0; PTC Inc., Needham, MA, USA) to evaluate the fitness (gap distances) between AATBP and three normal patellae on the inferior surface. The AATBP midline and each patella were aligned first. The total height (proximal–

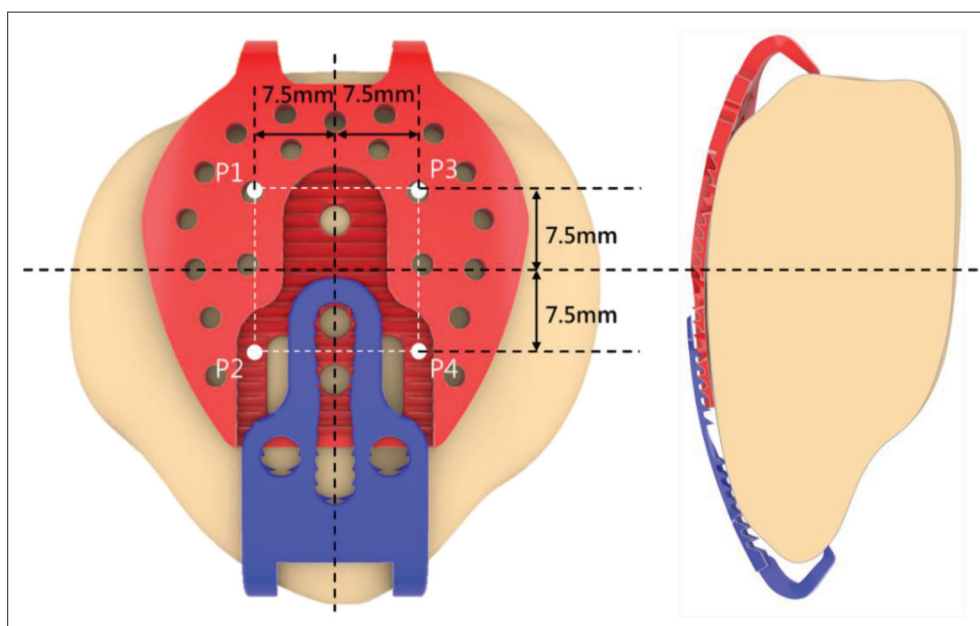


Figure 3. Illustration of the gap distance measurement between the AATBP and the patella at the positions of the four vertices of a 15 mm × 15 mm square in the AATBP center.

distal direction) of the AATBP was adjusted using its attached ratchet to allow two pairs of hooks to grip at relative positions on the proximal and distal ends of the three patellae. The gap distances between the AATBP and each patella at four vertices of a 15 mm × 15 mm square defined the AATBP center (Figure 3).

2.2. AATBP 3D printing

The AATBP without screw holes was manufactured using selective laser melting of a metal powder bed fusion machine (AM250; Renishaw, Wotton-under-Edge, UK), noted as a 3D printing system with commercial titanium alloy powder (diameter of Ti6Al4V powder ranges between 15 μm and 45 μm). The 3D printing system was operated at a laser power of 400 W, a scanning rate of 0.6 m/s, and an exposure time of 125 s^[13]. The metal powder was selectively scanned and melted by a laser during the process. The component was complete after the powder was crystallized. In the present study, the manufacturing accuracy, hatching space, and layer thickness were 30, 90, and 30 μm, respectively. The 3D-printed AATBP surface burring without screw holes was removed and polished using a magnetic polisher with stainless steel pins (Ø = 1 mm, L = 3 mm) at a speed of 2,700 rpm. The device was then cleaned using ultrasonic oscillations (Figure 4)^[13].

There were high demands for screw holes with thread accuracy down to 0.02 mm and screw hole surface without cracks. All PP and DP screw holes were generated using traditional XXX (CNC) positioning drilling to control the manufacturing accuracy within a small error margin

and enable the commercial screw to fit the hole within an acceptable error range.

Our 3D printer and CNC machining laboratories were certified under the Good Manufacturing Practice (GMP) quality management system (Certificate Number: QMS0940; A Plus Biotechnology Co. Ltd, Taipei, Taiwan). This ensured that the bone plate manufactured using 3D printing and CNC drilling can provide a practical foundation for approaches that meet GMP regulations, such as printing biocompatible materials in a biologically safe manner to meet the ISO10993 standard, as well as demonstrating a commitment to safety and quality.

The AATBP in this study was designed using computer-aided design (CAD) software. The detailed dimensions of all AATBP features in the CAD software were defined as the actual dimensions. The height, width, and thickness dimensions of the PP and DP as well as the ratchet and cone height pitch (shown in Figure 5 and defined in Table 1) were measured using a precision measuring system (ARCS Precision Technology Co., Ltd., Taiwan) on three randomly selected AATBP samples and compared with the corresponding actual values. We defined that the error for each dimension to be within 5%, namely the printed accuracy of our assembly bone plate should meet the requirements for implant manufacture.

2.3. AATBP bending strength and surface roughness tests

To provide a comprehensive mechanical strength reference for the AATBP used in the patella fracture cases, four-point



Figure 4. (a) 3D-printed AATBP prototypes without screw/wire holes and (b) 3D-printed AATBP with back cone bump after screw/wire holes generation by CNC machining.

bending tests were carried out according to the American Society for Testing and Materials (ASTM) protocols (ASTM F382-17), which are the main reference methods for FDA-approved bone plate functional testing^[14].

Static testing was performed using the Instron E10000 testing machine (INSTRON, Canton, MA, USA) to obtain the sample proof load and bending strength (Figure 6). The

rigid extension segments used to effectively lengthen the bone plate due to the AATBP do not have a symmetrical section and require a sufficiently long symmetrical section. The geometric profile at the proximal and distal sides of the rigid extension segments for the AATBP were designed according to geometric features of their corresponding contact bone plate and fabricated using a metal 3D printer.

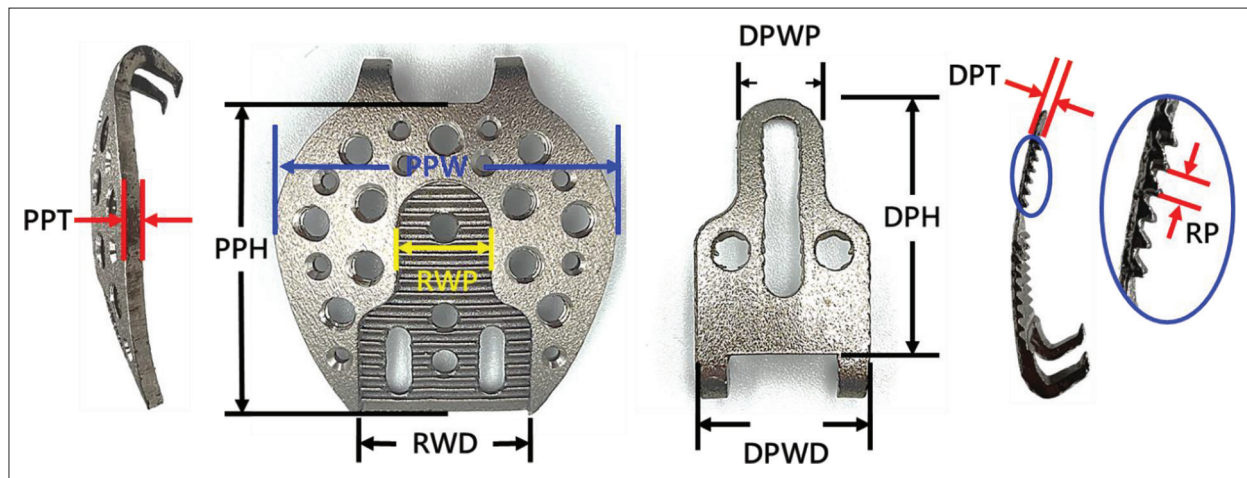


Figure 5. Illustration of all detailed dimensions.

Abbreviations: PPT: proximal plate thickness; PPW: proximal plate width; PPH: proximal plate height; RWP: ratchet width in the proximal side; RWD: ratchet width in the distal side; DPH: distal plate height; DPWP: distal plate width in the proximal side; DPWD: distal plate width in the distal side; DPT: distal plate thickness; RP: ratchet pitch.

Table 1. Detailed dimension verification between 3D printed manufacturing and CAD (true) for AATBP

Item	PPT	PPW	PPH	RWP	RWD	DPH	DPWP	DPWD	DPT	RP
CAD	1.60	34.3	32.3	9.40	17.6	25.6	8.30	16.5	0.43	1.30
3DP (Avg.)	1.66	34.4	32.1	9.50	17.5	25.5	8.50	16.6	0.44	1.32
Abs error (%)	3.75	0.29	0.62	1.06	0.57	0.39	2.41	0.61	2.33	1.54

Unit: mm

Abbreviations: 3DP: 3D printing; CAD: computer-aided design; PPT: proximal plate thickness; PPW: proximal plate width; PPH: proximal plate height; RWP: ratchet width in the proximal side; RWD: ratchet width in the distal side; DPH: distal plate height; DPWP: distal plate width in the proximal side; DPWD: distal plate width in the distal side; DPT: distal plate thickness; RP: ratchet pitch.

The bone plate was fixed onto the corresponding rigid extension segments, and the loading rollers contacted the rigid extension segments of the test setup during the test (Figure 6). Center span (a) is the distance between the loading rollers, and the loading span distance (h) is the distance between the loading roller and nearest support roller. The corresponding distances for a and h for the AATBP were both 40 mm (Figure 6). Three samples were placed on the four-point bending test clamp to load at a cross-head rate of 0.05 mm/s until failure occurred. The proof load (P) (the intersection line of a 0.2% offset from the linear portion of the load–displacement curve) and the bending strength were obtained from multiplying the proof load by the loading span distance (h) and dividing by 2 ($P \times h/2$), according to the ASTM F382 standard test method. The failure pattern for each sample was examined visually to assess the failure mechanism (Figure 6).

Surface roughness (Ra) on the three AATBPs randomly selected from all plates were measured on the L1, L2 (interior surface), and L3 (posterior surface) segments of PP and L4 (interior surface) segment on the DP using a portable measuring instrument with $6 \times 10^{-3} \mu\text{m}$ resolution

(SJ-210, Mitutoyo Co, Ltd., Tokyo, Japan) to understand the surface roughness of 3D-printed components (Table 2).

2.4. Biomechanical static/dynamic testing

3D CAD models of the patella and corresponding femoral condyle reconstructed from Sawbone CT images were fabricated using a 3D printer (Dimension 1200es SST; Stratasys, Ltd., Eden Prairie, MN, USA) with acrylonitrile butadiene styrene (ABS) material (ABS-P430; Stratasys, Ltd.). Fifteen ABS patellae were identically osteotomized horizontally in the center to mimic a transverse fracture and passed through a polyester tension belt (25 mm in width) loop, which plays the role of quadriceps and patellar tendons. The fractured patellae were divided randomly into three groups (5 per group) to perform the static/dynamic biomechanical tests for conventional TBW and the dynamic AATBP fixations, as described below according to the groups.

For the TBW fixation sample, two K-wires (Syntec Scientific Co., Taiwan) of 2.0 mm in diameter were inserted orthogonally into the patella osteotomy plane and parallel to each other on its medial 1/3 and lateral 1/3. The roll

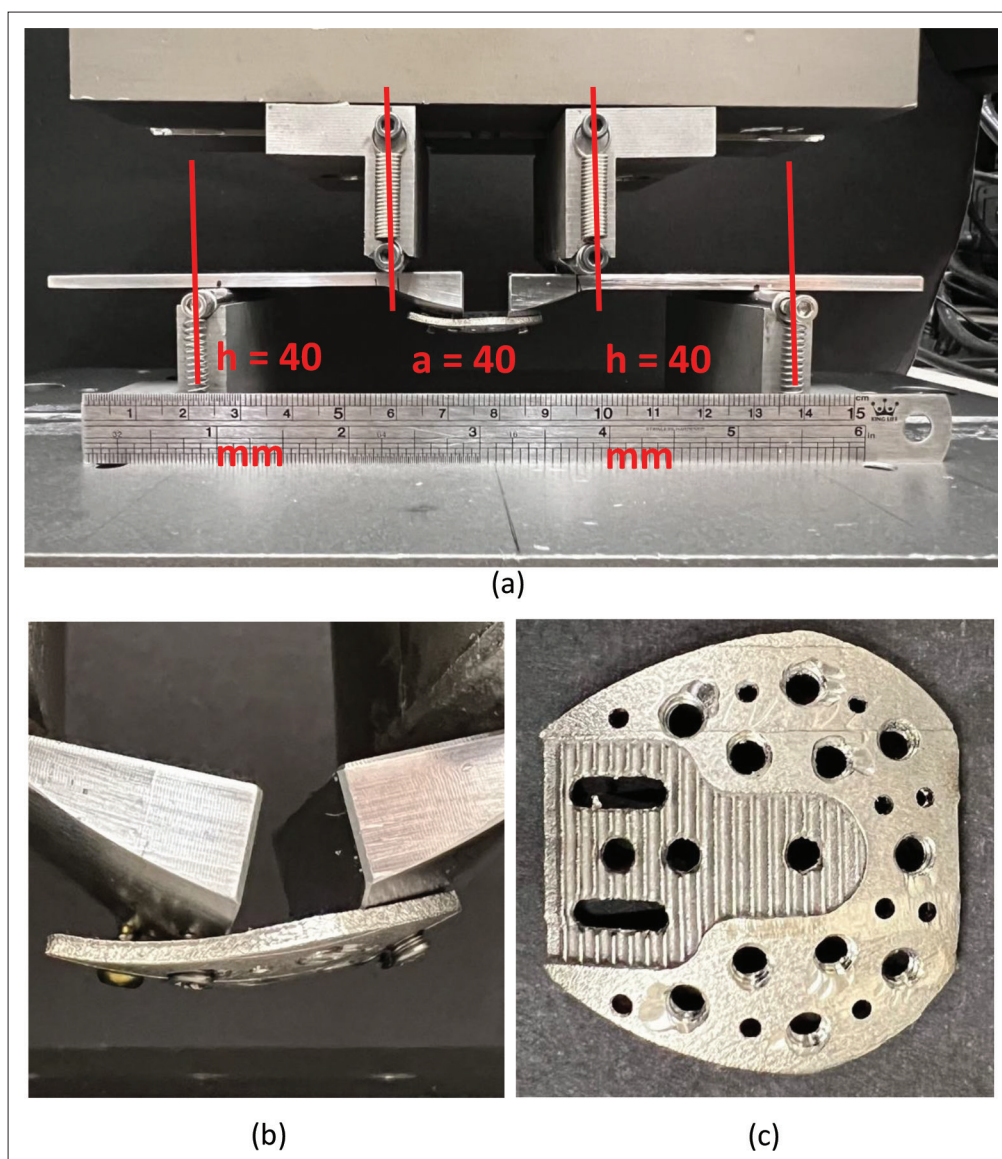


Figure 6. (a) Illustration of the four-point bending test according to ASTM F382; the AATBP was fixed onto the corresponding rigid extension segments; the loading rollers contacted the rigid extension segments of the test setup during the test; (b) locking screw loosening after test; and (c) the position of the AATBP damage.

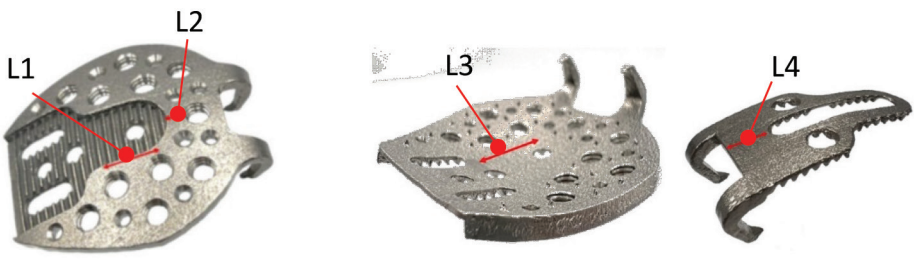
wire loop (Syntec Scientific Co., Taiwan) with a diameter of 1.25 mm was laid around the protruding K-wire ends, forming a figure-of-eight on the patella anterior surface. Two knots were twisted into the distal part of the K-wire and tightened. The proximal part of the K-wire was bent, cut, and impacted to ensure its complete contact with the ABS bone surface (Figure 7a)^[15].

For AATBP fixation, PP and DP were adjusted to the assembly using a ratchet mechanism for fitting the patella height (about 46.8 mm) and holding the fractured fragments by the corresponding hook pairs passing through the belt. The AATBP curved surface can be adjusted as

much as possible to coincide with the anterior curved surface of the patella before being secured. Five locking and three compressive screws of 2.4 mm in diameter (A Plus Biotechnology Co. Ltd, Taipei, Taiwan) distributed with medial-lateral symmetry were inserted into PP and DP, respectively, to fix the fractured patella. These screws spanned the fracture gap (Figure 7a).

To evaluate the PP and distal DP assembly flatness through the ratchet teeth, three AATBPs were randomly selected and erected to allow the anterior surface to be positioned parallel to the ARCS light source. This allowed assembly tightness error measurement between the two

Table 2. Surface roughness measured positions for the AATBP and corresponding obtained results



Sample 1	4.135	5.960	5.454	3.323
Sample 2	4.427	5.495	4.438	3.545
Sample 3	4.698	5.325	6.264	3.824
Mean ± Std (µm)	4.42 ± 0.28	5.59 ± 0.33	5.39 ± 0.91	3.56 ± 0.25

Unit: µm

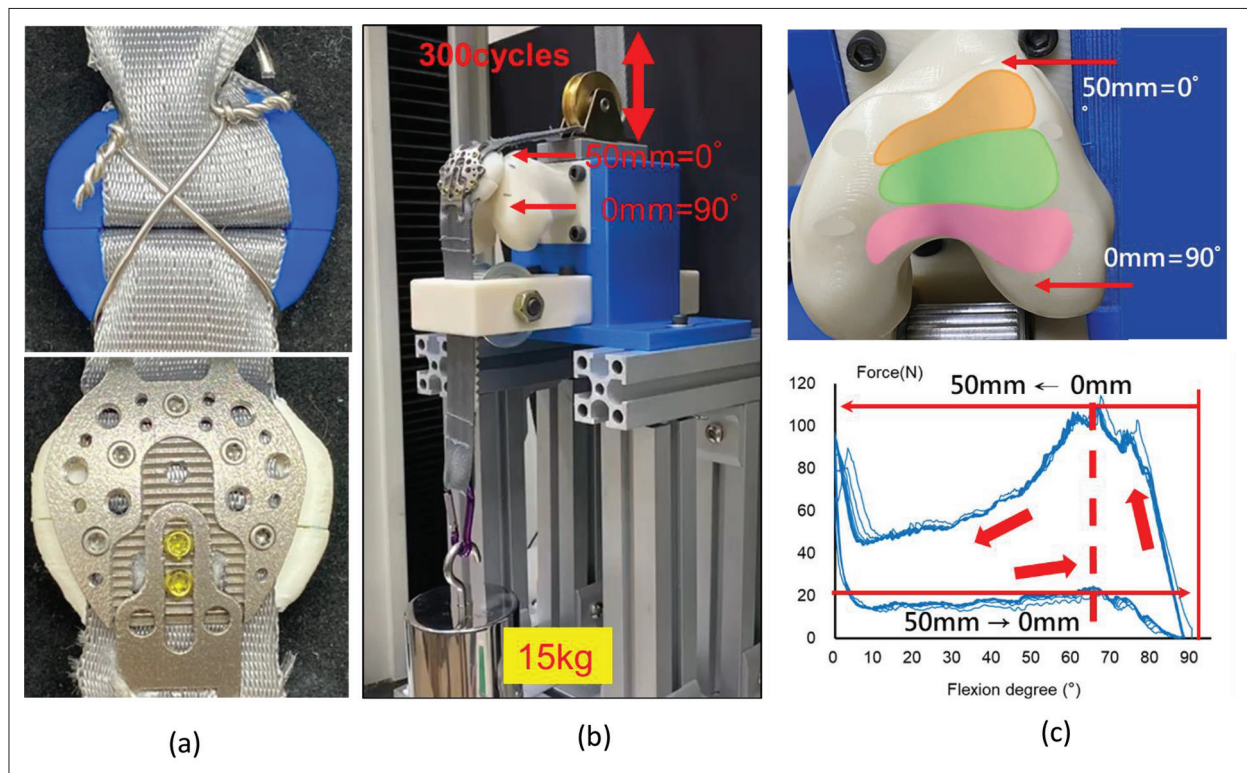


Figure 7. (a) Samples using TBW (top) and AATBP (down) fixation for fractured patella. (b) Dynamic biomechanical testing device. (c) Position-controlled stroke of corresponding femur contact positions (top) from 0° to 90° (50 mm to 0 mm) knee flexion and back to 0° (0 mm to 50 mm) (down) extension in each cycle at a constant velocity.

thin bone plates at the proximal and distal positions (Figure 8).

Five TBW and one AATBP fixation samples were clamped vertically on the Instron machine. A 20 N preload was necessary to reflect the fact that the tension belt loop needed to be extended to a point at which a linear increase in the force–displacement diagrams could be observed.

Static tensile failure tests on each sample were performed with 5 mm/min speed until the fracture gap exceeded 2 mm, and the force–displacement diagram was recorded. Note that the force corresponding to the region in the diagram has volatility.

For the dynamic tests, all patellae were evaluated in simulated 90° knee flexion to 0° full extension using a

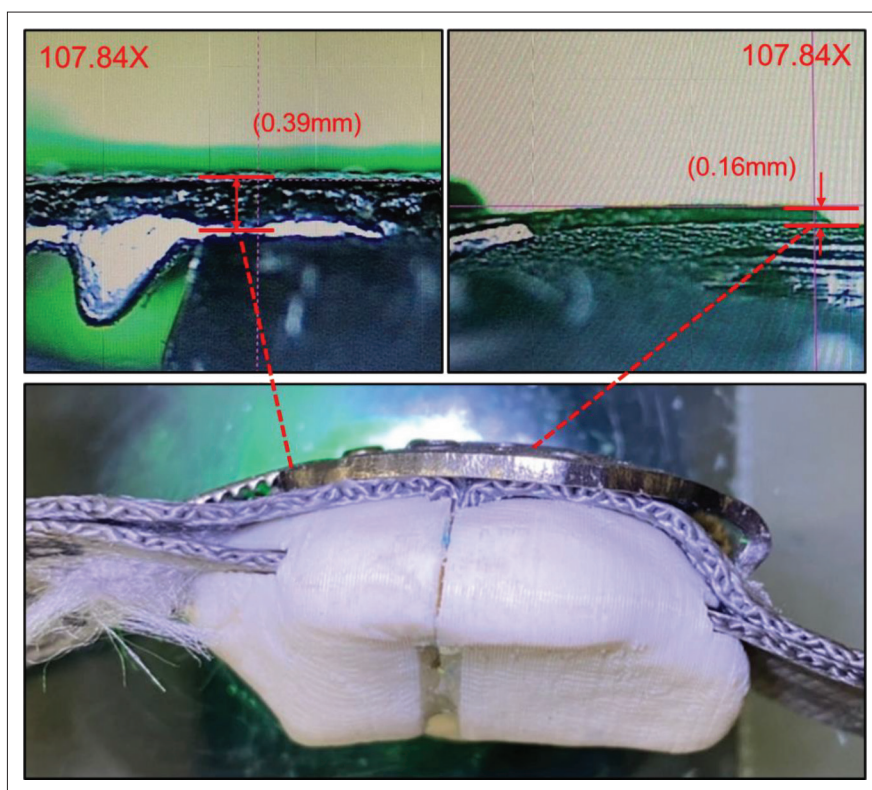


Figure 8. Assembly tightness error measurement between the PP and DP at the proximal (top-right) and distal positions (top-left).

printed ABS femur condyle as a pivot point following the biomechanical model from the literature (Figure 7b and c)^[2,3,4,16]. Tension was applied via the previously attached polyester belt loop, and corresponding proximal (quadriceps tendon) and distal (patella tendon) belts were connected to the Instron load cell and the 15-kg (about 150 N) vertical downward weight, respectively. Each cycle load test simulated the patella–femur contact positions from 90° knee flexion (set travel distant was 0 mm) and back to 0° full extension (travel distant was 50 mm) with a constant velocity of 5 mm/s. Another five TBW and AATBP fixation samples were tested subsequently for 300 cycles by carrying out a position-controlled (50 mm) stroke. The quadriceps tendon force obtained from the load cell relative to flexion–extension stroke displacement in each load cycle was recorded and plotted (Figure 7c). In addition, the fracture gap was measured at the medial and lateral border of each patella before and after the last testing cycle using a digital caliper.

2.5. Finite element analysis

The 3D CAD models of the transverse fracture patella matched the conventional TBW (included K-wire and figure-of-eight roll wire loop), and the AATBP fixations were generated and imported into the ANSYS Workbench (V18, Swanson Analysis, Houston, Pennsylvania, USA).

Two FE models of the transverse fracture patella fixed with TBW and AATBP were generated with quadratic 10-node tetrahedral structural solid elements and a total of 44099/181769 elements and 72721/314783 nodes for TBW/AATBP models, respectively (Figure 9). Frictional contact elements with different coefficients of friction were adopted from the literature to simulate the contact behaviors on bone–bone (at the fracture site), AATBP–bone, and wire–bone surfaces^[17–20]. The corresponding values were 0.45, 0.3, and 0.3, respectively. Cortical, cancellous bones, AATBP, fixation screws, and K-wire were defined with linear elastic and isotropic properties adopted from the relevant literature. The wire loop material property was considered as a bi-linear hardening plastic behavior to mimic the permanent deformation of stainless wire, and the yield stress and tangent modulus were also adopted from the literature^[17–20].

Nodes on the patella proximal side (base) were constrained in all directions as the boundary conditions. A tension force of 150 N similar to the load condition in the biomechanical test was applied to the patellar apex parallel to the long axis to mimic patella tendon force (Figure 9)^[17–20]. The articulating part of the distal femur was not taken into account in this FE analysis, and thus, relevant data was obtained from the literature^[17–20]. The inferior patella

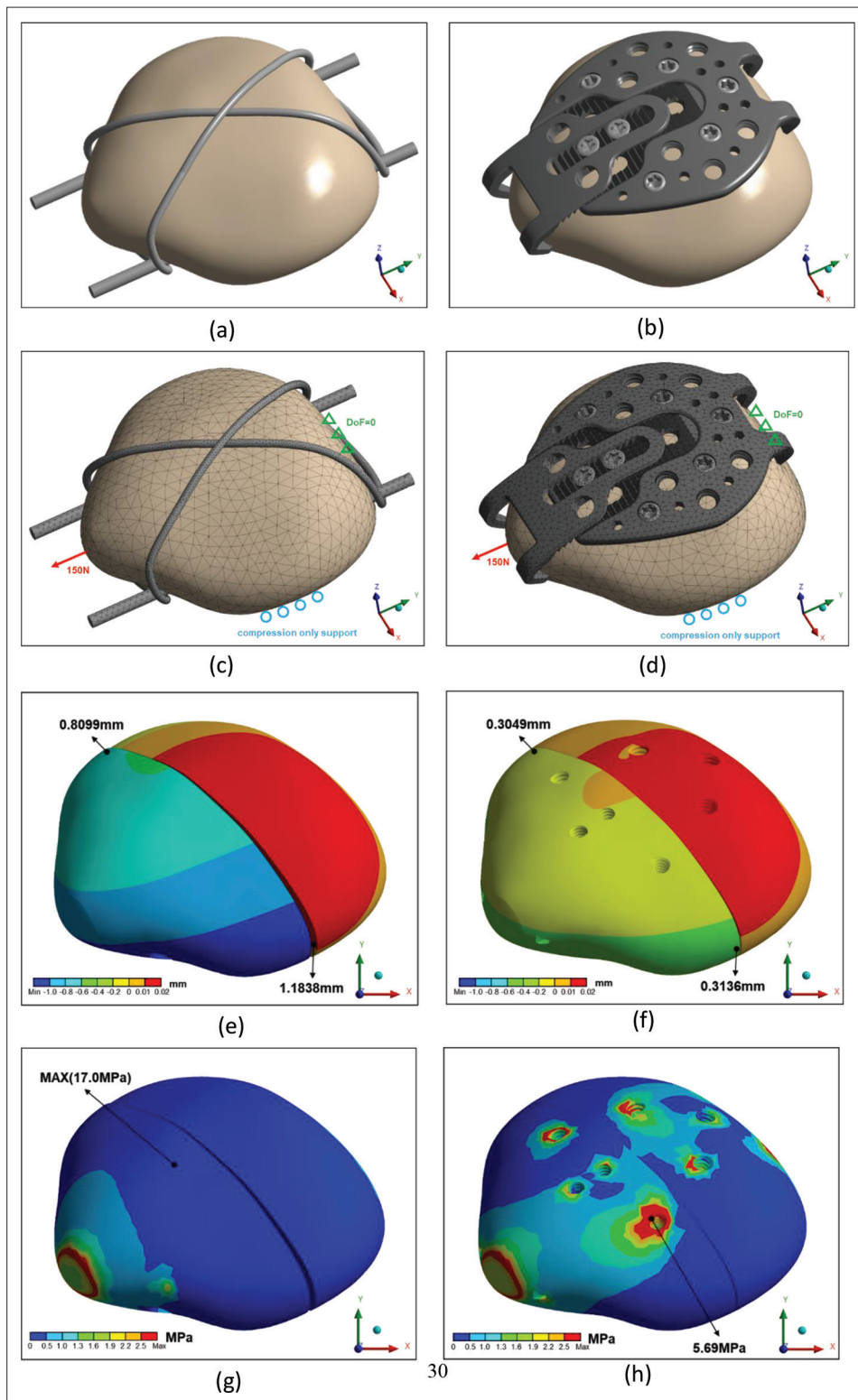


Figure 9. (a) The solid mode for TBW fixation; (b) the solid model for AATBP fixation; (c) the mesh model for TBW TWB fixation; (d) the mesh model for AATBP fixation; (e) simulated displacement result for TBW fixation; (f) simulated displacement result for AATBP fixation; (g) simulated von Mises bone stress result for TBW fixation; and (h) simulated von Mises bone stress result for AATBP fixation.

Table 3. Results of the mean (standard deviation) gap distances between AATBP and each of the patella surfaces at the positions of the four vertices (P1, P2, P3, and P4)

	P1	P2	P3	P4
Sample 1	0.50	0.41	0.09	1.01
Sample 2	0.30	0.73	0.11	1.14
Sample 3	1.36	0.16	0.49	0.57
Mean \pm Std (mm)	0.72 \pm 0.46	0.43 \pm 0.23	0.23 \pm 0.18	0.91 \pm 0.24

Unit: mm

surface was defined as a compression-only support in analysis that enables the surfaces to only bear compression and not tension forces to mimic support from distal femur condyles (Figure 9). The fractured gap distances at the medial and lateral sides for two fixation models and maximum von Mises strain of bone around the screw hole were recorded.

3. Results

3.1. Design and 3D printing feasibility analysis

The mean (standard deviation) gap distance results between the AATBP and each of the patella surfaces at the positions of the four vertices (P1, P2, P3, and P4) of the 15 mm \times 15 mm square for the three patellae were 0.72 \pm 0.46 mm, 0.43 \pm 0.23 mm, 0.23 \pm 0.18 mm, and 0.91 \pm 0.24 mm (Table 3). The AATBP manufacturing errors were both within 5% (maximum error of 3.75%), which showed that the metal 3D printing equipment used in this study has good precision and was suitable for medical applications (Table 1). The assembly tightness errors between the PP and DP at the proximal and distal positions were only 0.34 and 0.17 mm, respectively (Table 4).

3.2. AATBP bending strength and surface roughness

In the static four-point bending test, the values of the average proof load and bending strength for AATBP were 58.38 \pm 4.51 N and 1167 \pm 90.39 N \cdot mm, respectively. The failure mode of the AATBP after static tensile test showed that the plate was damaged around the screw holes because screws were pulled out from the rigid extension segment (Figure 6b and c). The surface roughness test results showed that the mean (standard deviation) surface roughness for L1, L2, L3, and L4 segments were 4.42 \pm 0.28 μ m, 5.59 \pm 0.33 μ m, 5.39 \pm 0.91 μ m, and 3.56 \pm 0.25 μ m, respectively (Table 2).

3.3. Biomechanical static/dynamic testing

The static test for TBW fixation found that the average fractured gap distance before and after the cyclic loads was 3.06 \pm 1.97 mm (>2 mm), and the corresponding force was 351.98 N. The average force of the region with a volatility in the force–displacement curve was recorded

Table 4. Results of the assembly tightness error between the PP and DP

Sample	Assembly tightness error between PP and DP	
	Proximal side (mm)	Distal side (mm)
1	0.39	0.16
2	0.31	0.15
3	0.33	0.20
Mean \pm Std (mm)	0.34 \pm 0.04	0.17 \pm 0.03

Unit: mm

as 143.58 N (Figure 10). In contrast, the AATBP fixation force–displacement curve was found to be smooth until tensile testing stopped. The dynamic test results showed that the average fractured gap distances at the medial/lateral sides before and after cyclic load testing were 2.38 \pm 0.57 mm/2.30 \pm 0.30 mm for TBW and 0.03 \pm 0.01 mm/0.06 \pm 0.03 mm for AATBP fixations (Table 5). This showed that the variations in the fractured gap distances were significantly different between TBW and AATBP, irrespective of whether the medial or lateral side was analyzed, with all $p < 0.05$ using the Kruskal–Wallis test because sample sizes were relatively small, and it could not be determined whether the data were normally distributed. Figure 11 shows all samples fixed with TBW/AATBP after dynamic testing to show the fracture gaps, and we found no sustained damage on the AATBPs.

3.4. Finite element analysis

The FE analysis result showed that the fractured gap distances at the medial/lateral sides for TBW and AATBP fixation models were 0.8099 mm/1.1838 mm and 0.3049 mm/0.3136 mm, respectively. The AATBP fixation fracture gap was found obviously smaller than those of TBW fixation under receiving tensile loads regardless of medial or lateral sides. The maximum von Mises stress of the bones were found around the medial wire hole and lateral bottom locking screw hole for TBW and AATBP fixations, respectively (Figure 9). The corresponding value for TBW fixation was 17 MPa and much higher than that of 5.69 MPa for AATBP fixation. Nevertheless, both bony stress values were a lot smaller than the bone fracture strength.

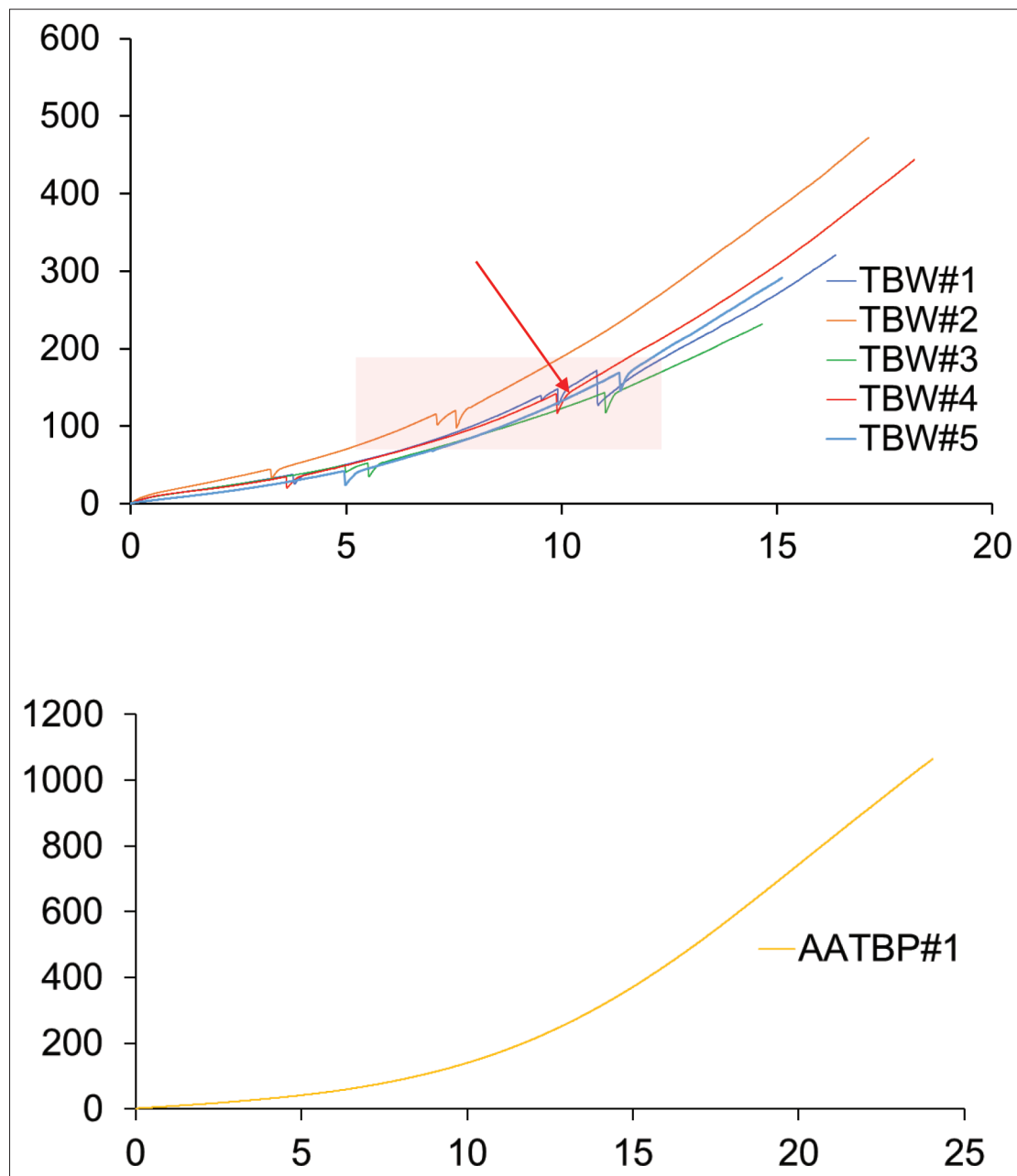


Figure 10. Static test force–displacement curves for TBW (top) and AATBP (down) fixations.

4. Discussion

It has been clearly shown that a fixation bone plate for transverse patella fractures was more stable than those using only band wires and screws combined with band wires from the literature^[3,4]. However, a suitable design for the fixation bone plate needs to be relatively complicated in order to achieve the various functions necessary for fulfilling unmet clinical needs. This cannot be achieved using traditional manufacturing processing. The AATBP proposed in this study included two anatomical thin plates

with a hook mechanism to hold fractured fragments, a ratchet mechanism to adjust plate height, and cone bumps at the plate base to enhance retention. Therefore, traditional processing methods, even those using five-axis CNC machines, may not be able to meet such complex manufacturing requirements. Precise 3D printing is needed to manufacture the AATBP.

The fixation bone plate should be designed to fit the patella anterior surface as much as possible to restore the fractured bone correctly since it has a curved contour.

Table 5. Results of variation in the fractured gap distances at the medial/lateral sides before and after dynamic tests and corresponding maximum forces

Fixation	Sample	Medial side (mm)	Lateral side (mm)	Maximum force (N)
TBW	#1	2.05	2.26	320
	#2	3.4	2.81	427.25
	#3	2.16	2.24	292.5
	#4	2.13	2.06	330
	#5	2.17	2.11	318.15
	Mean \pm Std	2.38 \pm 0.57	2.30 \pm 0.30	337.58 \pm 52.00
AATBP	#1	0.03	0.1	262.25
	#2	0.02	0.02	271.25
	#3	0.03	0.08	238.13
	#4	0.03	0.04	242.13
	#5	0.04	0.05	260.52
	Mean \pm Std	0.03 \pm 0.01	0.06 \pm 0.03	254.86 \pm 14.12

The titanium alloy bone plate with ductile material properties can be bent during the surgical process when the plate is manufactured using a traditional cutting method. However, the bone plate is no longer bendable and exhibits brittleness when the manufactured process is changed to 3D printing. The design accuracy for the curved surface becomes more important. The AATBP anatomical anterior surface was obtained by capturing the Sawbone patella surface, and it was confirmed that this bone plate surface shape design is feasible since the largest gap distance between the AATBP and the normal patella surface is only 0.91 mm.

Since there is no comparable fixation bone plate mechanical strength for patella fractures, the proof load and bending strength of the commercial dorsal fixation bone plate for distal radius fracture obtained using the same testing method according to ASTM F382 were selected as the comparable index to identify the mechanical capability of our AATBP. The proof load and bending strength were 47.36 ± 5.36 N and 1183 ± 134 N·mm obtained from the literature^[21]. Since the center span (a) and the loading span distance (h) of these two bone plate tests were different, bending strength was only compared, and we found that there was no significant difference between the radius dorsal fixation plate and the AATBP. This implied that the mechanical strength of the AATBP developed in this study met the clinical needs. For the surface roughness compression, the average surface roughness of an oblique lumbar interbody fusion cage used in this study was $9.143 \mu\text{m}$, which is from literature^[22]. This value was about 1.92 times ($9.143 \mu\text{m}/4.74 \mu\text{m}$) the AATBP average roughness measured [$(4.42 + 5.59 + 5.39 + 3.56)/4 = 4.74 \mu\text{m}$] in this study. This phenomenon also showed that the surface roughness of the components manufactured by 3D printing fell within a reasonable range.

The most important issue in AATBP 3D printing is that the assembly tightness error of the two thin bone plates at the proximal and distal ends must be minimized. The ratchet manufacturing must be sufficiently accurate to allow assembly surface flatness control within the unsuitable skin touch feeling range. The maximum value for the average tightness error for two thin bone plate assemblies was only 0.34 mm when produced by our metal 3D printing machine, with values of $30 \mu\text{m}$ for both the manufacturing accuracy and the layer thickness. This value cannot be perceived through the touch with hand and is also less than the total thickness of 1.6 mm for the AATBP. This implies that a similar assembly bone plate design can be fabricated when the manufacturing accuracy requirement for the metal 3D printing machine is less than $30 \mu\text{m}$.

Commercial locking and compressive bone screws were selected to match our AATBP because bone screws did not need to be manufactured by 3D printing. This is beneficial for reducing manufacturing cost, time, and accuracy requirements. In the traditional manufacturing process, the required accuracy for bone screws can be 0.02 mm, with relatively good ductility and suitability for a large allowable rotation angle for bone insertion. However, the 3D printing manufacturing process usually confers a tendency for the material to be brittle and not suitable for bone screw manufacturing when no special post-processing is performed. We therefore only tapped threads or drilled holes into our AATBP using five-axis machining for the corresponding bone screw insertion.

Fifteen-kilogram downward weights were applied on the dynamic cyclic loads because a volatility in force was found at the critical value in the force–displacement curve during the static test for TBW fixation. This implied that

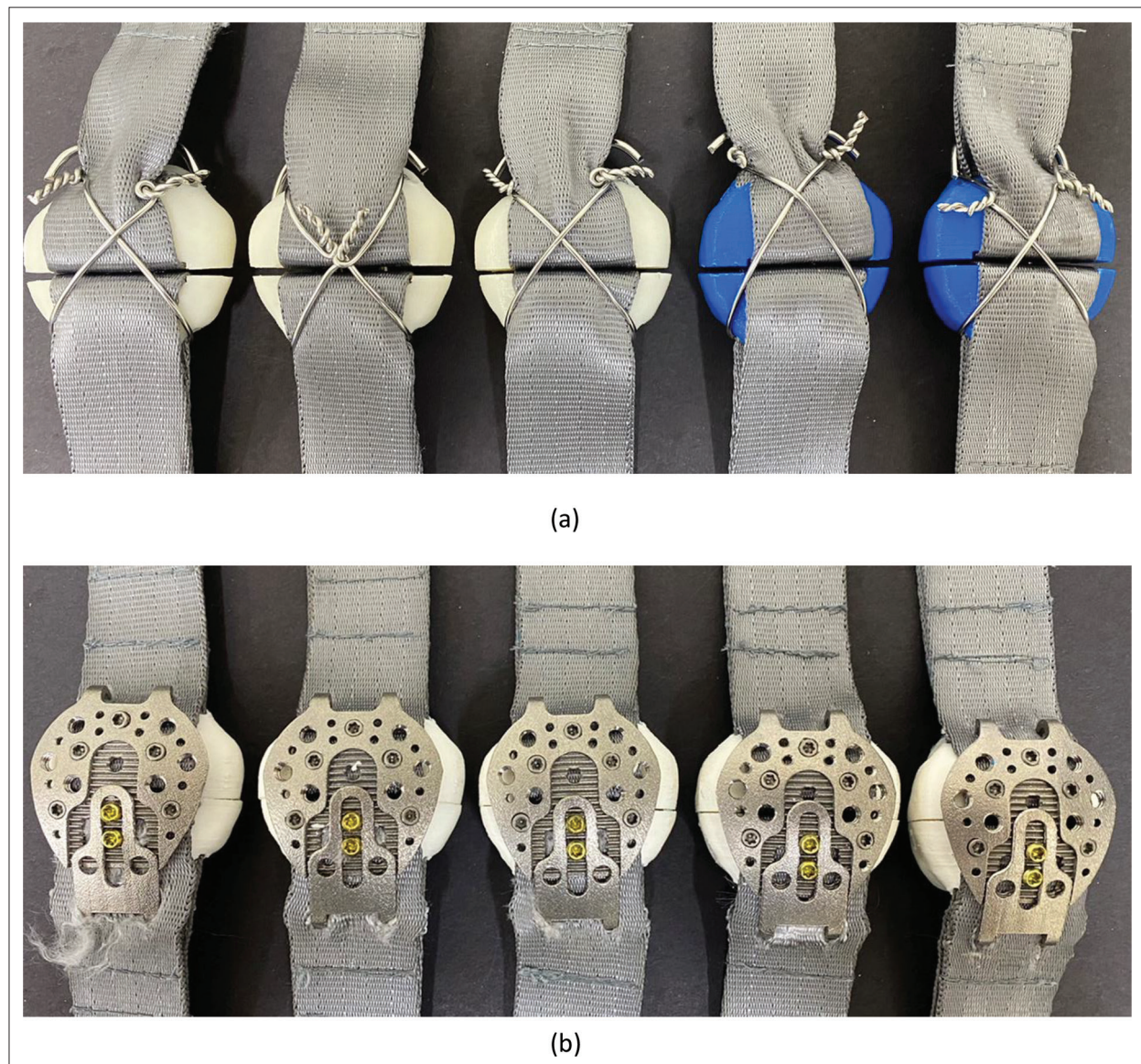


Figure 11. The fractured gap distances at the medial/lateral sides and situations for all fixation patella samples after cyclic tests for (a) TWB and (b) AATBP fixations.

the fractured patella was starting to become unstable. A biomechanical test platform as described in the literature was set up to evaluate the dynamic biomechanical behavior of the fractured patella after TBW and AATBP fixations^[2-5]. The force test results showed that the maximum force can be obtained at an extension angle of 60° (Figure 7c), which is consistent with the literature reporting the motion pattern of the knee joint. This also means that this platform can be used in similar tests in the future^[23]. The results showed that the corresponding force at 60° was 254.86 ± 14.12 N for AATBP and 337.58 ± 52.00 N for TBW fixation. This clearly indicated that the conventional TBW fixation cannot hold on to the fractured patella fragments and

that the quadriceps tendon needs to bear greater force to maintain the fixation system balance.

The fracture gap distance results at the medial/lateral sides before and after the dynamic test showed that the fractured patella stability after fixation was greater and the gap distances were approximately zero when 3D-printed AATBP fixation was used. This was almost 75 (2.24 mm/0.03 mm) times less for the medial direction and 40 (2.30 mm/0.06 mm) times less for the lateral direction than when using TBW fixation. This is reasonable because the fractured patella proximal and distal fragments were effectively grasped by the hooks and forced into the fractured gap.

The patella fragments were also fixed by bone screws and AATBP. This was clearly different from the fixation using TBW without holding power and suggested that AATBP can be further applied to *in vivo* tests.

The FE simulation and biomechanical test results showed the same trend, i.e., fractured gap distances at the medial/lateral sides for TBW were both higher than that of AATBP fixation models. The TBW fixation cannot hold the fracture segments of the patella efficiency, and the maximum bone stress found around the medical wire inserted into the patella might cause the fracture segments to slide. The bone stress concentration for the AATBP fixation was found around the screw. The corresponding maximum stress value was 5.69 MPa and at the lateral bottom screw hole. Although the maximum stress value was much lower than the tensile ultimate strength (135 MPa), it should be noted that it may cause locking screw loosening^[24].

The patella fracture types are not limited to transverse fractures but also include other forms of comminuted fractures or proximal/distal fractures. The main objective of surgical treatment is to restore these comminuted bones to their original anatomical positions while maintaining their stability. A fixation bone plate designed to have good encircling energy (holding power) for the fractured patella is recommended. Our AATBP and the experimental/simulation results presented herein manifest this property and can be applied to the main patella fracture of the transverse type, as well as other fracture forms in the future.

Although the AATBP was designed with an anatomical contour and has been confirmed to be adaptable for use, this bone plate may not enable clinicians to do much manual bending during surgery due to the limitations of 3D-printed materials and post-manufacturing processing. More rigorous *in vivo* experiments may be required to further confirm the clinical utility of the AATBP, although the biomechanical stability was confirmed in this study.

5. Conclusion

This study confirmed that the thin structural bone plate for patella fixation, comprising anatomical surface, hook, small cone, and size-adjustable ratchet mechanism, can be fabricated using 3D metal printing with acceptable manufacturing error and reasonable anatomical surface/thin bone plate assembly fitness, mechanical bending strength, and surface roughness. The biomechanical cyclic test results showed that the fracture gap between two AATBP fixation fracture segments after cyclic loads was smaller and superior to conventional TBW for patella transverse fractures. The FE simulation result addressed the stress concentration around the screw holes and noted the high risk for screw loosening.

Acknowledgments

None.

Funding

This study is supported in part by MOST project 108-2622-E-010-001-CC2 and 110-2222-E-032-003-MY2, Taiwan.

Conflict of interest

The authors declare no conflicts of interest.

Author contributions

Conceptualization: C.Y. Liao, Chun-Li Lin

Investigation: Shao-Fu Huang, Wei-Che Tsai, Yu-Hui Zeng, Chia-Hsuan Li

Methodology: Chun-Li Lin

Writing – original draft: C.Y. Liao, Chun-Li Lin

Writing – review & editing: C.Y. Liao, Chun-Li Lin

Ethics approval and consent to participate

Not applicable.

Consent for publication

Not applicable.

Availability of data

Not applicable.

References

1. Lee KH, Lee Y, Lee YH, *et al.*, 2019, Biomechanical comparison of three tension band wiring techniques for transverse fracture of patella: Kirschner wires, cannulated screws, and ring pins, *J Orthop Surg*, 27(3): 2309499019882140.
2. Gibert S, Kowaleski MP, Matthys R, *et al.*, 2016, Biomechanical comparison of pin and tension-band wire fixation with a prototype locking plate fixation in a transverse canine patellar fracture model. *Vet Comp Orthop Traumatol*, 29(1): 20–28.
3. Wild M, Eichler C, Thelen S, *et al.*, 2010, Fixed-angle plate osteosynthesis of the patella - an alternative to tension wiring? *Clin Biomech*, 25(4): 341–347.
4. Thelen S, Schnependahl J, Jopen E, *et al.*, 2012, Biomechanical cadaver testing of a fixed-angle plate in comparison to tension wiring and screw fixation in transverse patella fractures. *Injury*, 43(8): 1290–1295.
5. Thelen S, Schnependahl J, Baumgärtner R, *et al.*, 2013, Cyclic long-term loading of a bilateral fixed-angle plate in comparison with tension band wiring with K-wires or

- cannulated screws in transverse patella fractures. *Knee Surg Sports Traumatol Arthrosc*, 21(2): 311–317.
6. D'Ambrosio M, Tang A, Menken L, *et al.*, 2022, Adjunct neutralization plating in patella fracture fixation: A technical trick, *OTA Int*, 5(4): e217.
 7. Stoffel K, Zderic I, Pastor T, *et al.*, 2023, Anterior variable-angle locked plating versus tension band wiring of simple and complex patella fractures - a biomechanical investigation. *BMC Musculoskelet Disord*, 24(1): 279.
 8. Kumar G, Mereddy PK, Hakkalamani S, *et al.*, 2010, Implant removal following surgical stabilization of patella fracture. *Orthopedics*, 33(5): 301–304.
 9. Dargel J, Gick S, Mader K, *et al.*, 2010, Biomechanical comparison of tension band- and interfragmentary screw fixation with a new implant in transverse patella fractures. *Injury*, 41(2): 156–160.
 10. Wagner FC, Neumann MV, Wolf S, *et al.*, 2020, Biomechanical comparison of a 3.5 mm anterior locking plate to cannulated screws with anterior tension band wiring in comminuted patellar fractures. *Injury*, 51(6): 1281–1287.
 11. Meda PVK, Machani B, Sinopidis C, *et al.*, 2006, Clavicular hook plate for lateral end fractures: A prospective study. *Injury*, 37(3): 277–283.
 12. Hung LK, Su KC, Lu WH, *et al.*, 2017, Biomechanical analysis of clavicle hook plate implantation with different hook angles in the acromioclavicular joint, *Int Orthop*, 41(8): 1663–1669.
 13. Chen CH, Chang WJ, Chen YS, *et al.*, 2022, Development of a novel hybrid suture anchor for osteoporosis by integrating titanium 3D printing and traditional machining. *Int J Bioprint*, 8(4): 608.
 14. Standard Specification and Test Method for Metallic Bone Plates, ASME F382-17
 15. Lee KH, Lee Y, Lee YH, *et al.*, 2019, Biomechanical comparison of three tension band wiring techniques for transverse fracture of patella: Kirschner wires, cannulated screws, and ring pins. *J Orthop Surg*, 27(3): 2309499019882140.
 16. Sharkey NA, Donahue SW, Smith TS, *et al.*, 1997, Patellar strain and patellofemoral contact after bone–patellar tendon–bone harvest for anterior cruciate ligament reconstruction. *Arch Phys Med Rehabil*, 78(3): 256–263.
 17. Chang CW, Chen CH, Li CT, *et al.*, 2020, Role of an additional third screw in the fixation of transverse patellar fracture with two parallel cannulated screw and anterior wire. *BMC Musculoskelet Disord*, 21(1): 752.
 18. Chang CW, Chen YN, Li CT, *et al.*, 2018, Role of screw proximity in the fixation of transverse patellar fractures with screws and a wire. *J Orthop Surg*, 26(3): 2309499018789705.
 19. Chen CH, Chen YN, Li CT, *et al.*, 2019, Roles of the screw types, proximity and anterior band wiring in the surgical fixation of transverse patellar fractures: A finite element investigation. *BMC Musculoskelet Disord*, 20(1): 99.
 20. Ling M, Zhan S, Jiang D, *et al.*, 2019, Where should Kirschner wires be placed when fixing patella fracture with modified tension-band wiring? A finite element analysis. *J Orthop Surg Res*, 14: 14.
 21. Liu HC, Zeng YH, Lin CL, 2021, Mechanical comparison of a novel hybrid and commercial dorsal double plating for distal radius fracture: In vitro fatigue four-point bending and biomechanical testing. *Materials (Basel)*, 14(20): 6189.
 22. Lai PL, Huang SF, Wang HW, *et al.*, 2023, Design an anatomical contour titanium 3D printed oblique lumbar interbody fusion cage with porous structure and embedded fixation screws for patients with osteoporosis. *Int J Bioprint* 9(5): 445–458.
 23. Bini RR, 2017, Patellofemoral and tibiofemoral forces during knee extension: simulations to strength training and rehabilitation exercises. *Fisioter Mov*, 30(Suppl 1): S267–5.
 24. Morgan EF, Unnikrisnan GU, Hussein AI, 2018, Bone mechanical properties in healthy and diseased states. *Annu Rev Biomed Eng*, 20: 119–143.